www.czasopisma.pan.pl PAN POLSKA AKADEMIA NAUK www.journals.pan.pl

Arch. Metall. Mater. **68** (2023), 2, 749-756

DOI: https://doi.org/10.24425/amm.2023.142457

D. BOLIBRUCHOVÁ[1], L. ŠIRANEC[1*], D. KAJÁNEK[2], M. CHALUPOVÁ[1]

MICROSTRUCTURE, MECHANICAL PROPERTIES AND CORROSION BEHAVIOR OF Zr-CONTAINING AlSi5Cu2Mg ALLOY

The aim of this paper was to analyze the impact of varying zirconium addition on selected properties of AlSi5Cu2Mg alloy. The results of this research showed that zirconium addition in the range of 0.05 to 0.20 wt. % caused a decrease in ultimate tensile strength and yield strength of the experimental alloys after T7 heat treatment, probably due to the formation of primary Al_3Zr intermetallic phases. These phases were observed as an individual plates or as a formation of two crossed plate-like phases. Potentiodynamic polarization tests in 3.5% NaCl solution revealed that addition of Zr had a positive effect on thermodynamic corrosion stability of the AlSi5Cu2Mg alloy due to shift of the corrosion potential to a more positive values for all as-cast samples. Addition of Zr in the as-cast alloys improved corrosion kinetics by lowering of corrosion current density.

Keywords: mechanical properties; zirconium; microstructure; corrosion; AlSi5Cu2Mg

1. Introduction

Age-hardenable Al-Si-Cu-Mg aluminum alloys are among the most widely used materials in the automotive industry. High strength-to-weight ratio, thermal stability, good castability and sufficient corrosion resistance are the main factors that make these alloys the first choice in the production of automotive engine parts, such as cylinder heads or engine blocks [1-3]. Modern automotive industry has been confronted with increasingly stringent environmental regulations in recent years. As a result, car manufacturers are therefore forced to reduce the weight of individual components while maintaining (or even enhancing) their utility properties. This approach requires close cooperation between automotive manufacturers and research centres in order to develop new types or aluminum alloys, or to substantially improve the alloys used so far [4-9].

In recent years, development in the field of aluminum alloy castings have focused on improving their properties by using alloying elements from the group of transition metals (Zr, Mo, V, Ni etc.). Of the transition metals, zirconium has gained popularity in the development of new types of aluminum alloys. The addition of Zr into the aluminum alloy is advantageous in terms of strength increase. The strengthening effect is induced by the crystallization of Zr-rich intermetallic phases (preferably the Al_3Zr phase). The Al_3Zr intermetallic phase can exist in two different crystallographic structures – metastable with cubic $L1_2$ structure and stable with tetragonal $D0_{23}$ structure. Zirconium has gained its popularity due to the formation of Al_3Zr phases with cubic $L1_2$ structure, which can act as potent nucleants for α (Al) phase and thus induce grain refinement of the microstructure [10-17].

Zirconium as an alloying element exhibit low diffusivity in Al matrix. Al_3Zr intermetallic phases are thus resistant to coarsening and dissolution, which makes them thermodynamically stable at elevated temperatures. This can be beneficial in maintaining the strength characteristics of the Al-Si-Cu-Mg aluminum alloys at elevated temperatures above 200°C, when Cu and Mg strengthening precipitates gradually coarse and dissolve. This results in a decrease in mechanical properties. Such a phenomenon is important to control in cylinder head castings of modern high-performance engines, which are exposed (especially in the area of the exhaust valves on the combustion part of the cylinder head) to temperatures exceeding 200°C [18-20]. Therefore, the use of Zr alloying element appears to be a convenient way to increase the thermal stability of newly developed aluminum alloys based on the Al-Si-Cu-Mg system.

The aim of this research was to study the effect of varying Zr addition on selected properties of Al-Si-Cu-Mg alloy. The subject of our research was non-standardized AlSi5Cu2Mg cylinder head aluminum alloy, which is new and has been used

[1] UNIVERSITY OF ŽILINA, FACULTY OF MECHANICAL ENGINEERING, UNIVERZITNÁ 8215/1, 010 26 ŽILINA, SLOVAKIA
[2] UNIVERSITY OF ŽILINA, RESEARCH CENTRE, UNIVERZITNÁ 8215/1, 010 26 ŽILINA, SLOVAKIA

* Corresponding author: lukas.siranec@fstroj.uniza.sk

in production for a relatively short time. Due to the specifically designed chemical composition, it is not possible to use standard AlTi5B1 grain refiner to refine the microstructure of this alloy. Therefore, it is necessary to find a suitable alloying element which would positively affect the microstructure and mechanical properties of this alloy. One possibility is to use Zr as an alloying element. As there is only a limited amount of information about this aluminum alloy, the research on the impact of Zr addition on selected properties appears to be appropriate for describing the properties of this alloy.

2. Material and methods

The aim of the experimental research was to determine the impact of varying Zr addition on selected properties of the AlSi5Cu2Mg alloy. It is a hypoeutectic aluminum alloy which is used in the automotive sector for the production of cylinder heads. Primary AlSi5Cu2Mg alloy was supplied in pre-modified state (via Sr addition) and without grain refinement, as the maximum permitted Ti content defined by the alloy's manufacturer is 0.03 wt. %. For an effective grain refinement of hypoeutectic aluminum alloys, 0.04 to 0.1 wt. % Ti content is required. A total of five experimental alloys with different Zr addition (0, 0.05, 0.10, 0.15 and 0.20 wt. % Zr) were produced for the experimental purposes. Chemical composition of the experimental alloys is given in TABLE 1. Zirconium was added to the experimental alloys via AlZr20 master alloy. Deteriorated solubility of the AlZr20 master alloy in the melt resulted in a lower actual Zr content in the experimental alloys with the addition of 0.15 and 0.20 wt. % Zr. The experimental alloys were cast into steel mold with temperature of 200±15°C by gravity casting. The mold was protected with a graphite coating.

TABLE 1

Chemical composition of the experimental alloys

Chemical composition [wt. %]									
Zr addition [wt. %]	**Si**	**Cu**	**Mg**	**Fe**	**Mn**	**Ti**	**Sr**	**Zr**	**Al**
0	5.47	1.91	0.29	0.18	0.02	0.013	0.01	**0.0009**	Bal.
0.05	5.67	1.91	0.29	0.19	0.02	0.013	0.01	**0.05**	Bal.
0.10	5.65	1.92	0.29	0.19	0.02	0.014	0.01	**0.10**	Bal.
0.15	5.55	1.91	0.29	0.19	0.02	0.014	0.01	**0.12**	Bal.
0.20	5.43	1.90	0.29	0.18	0.02	0.014	0.01	**0.19**	Bal.

The casting temperature was 745±5°C for all the experimental alloys. The experimental alloys were not degassed during their production. Ten samples were cast from each melt, of which five were intended for the evaluation of selected properties in as-cast state and five were evaluated in the state after heat treatment. The process of heat treatment was realized by T7 age hardening, consisting of solutionizing at 500±5°C for 6.5 hours, quenching into water with temperature of 80-90°C, artificial aging at 250±5°C for 4 hours followed by air cooling. T7 type is often used for heat treatment of engine parts such as cylinder heads in order to obtain a stable microstructure and mechanical behavior while operating at elevated temperature [21].

Evaluation of the mechanical properties was performed using an Inspekt desk 50 KN testing machine for tensile strength test according to ISO 6892-1 standard. A schematic representation of the tensile test bar specimen is shown in Fig. 1.

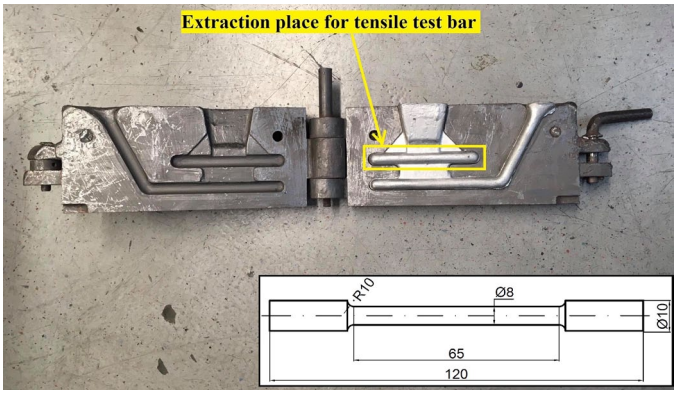

Fig. 1. Scheme of the tensile test bar showing the extraction place from the casting

Microstructure of the experimental alloys was observed using a NeoPhot 32 optical microscope and scanning electron microscope TESCAN LMU II with BRUKER energy-dispersive analyzer. Hardness of the experimental alloys was measured using a Brinell Innovatest Nexus 3000 hardness testing machine with ball indenter of 5 mm diameter, loading force of 250 kp (2451.6 N) and a load time of 10 seconds. Five locations for hardness measurement were selected on each experimental sample.

Corrosion behavior of the experimental alloys was evaluated using potentiodynamic polarization (PD) tests in 3.5% NaCl solution at laboratory temperature. Measurements were performed in three-electrode cell system on laboratory potentiostat Biologic SP300 with sample connected as a working electrode, Pt mesh as a counter electrode and saturated calomel electrode (SCE) served as reference electrode. Samples were examined using range of potentials from –200 mV to +500 mV vs. open circuit potential (OCP) with step rate of 1 mV/s after 10 min. of potential stabilization [22]. Measured PD curves were analysed using Tafel extrapolation method using EC Lab 10.42 software determining values of corrosion potential E_{corr}, corrosion current density i_{corr} and Tafel coefficients β_a and β_c determining anodic and cathodic slope of curves. Additionally, corrosion rate r_{corr} was calculated. Samples of the experimental alloys with varying Zr addition were sanded using a P1200 sandpaper before each PD test and measurements were repeated 5 times [23].

3. Results and discussion

3.1. Microstructure and fractography

Microstructural evaluation of the experimental alloys with varying Zr addition revealed the presence of α (Al) aluminum

matrix, modified eutectic Si and intermetallic phases based on Cu, Mg, Fe and Zr (Fig. 2a-e). Cu-rich intermetallic phases in the as-cast experimental alloys were observed in morphology of oval-shaped particles or as a ternary eutectic with compact morphology containing smaller oval particles. Fe-rich intermetallic phases were present in the experimental alloys as an acicular Al_5FeSi phase or as $Al_{15}(FeMn)_3Si_2$ phase with morphology of segmented skeletal structures.

Cu- and Mg- rich intermetallic phases dissolving occurred during solution heat treatment using the T7 heat treatment and a supersaturated solid solution was created during quenching into water. Further age hardening resulted in the precipitation of more uniformly dispersed precipitates within aluminum matrix, resulting in increased mechanical properties compared to the as-cast state. Spheroidization and clustering of eutectic Si particles (Fig. 3) occurred as a result of the T7 heat treatment.

Zr-rich intermetallic phases were found only in the experimental alloys with 0.15 and 0.20 wt. % Zr addition. The presence of Zr in these experimental alloys resulted in the formation of Zr-rich phases with plate-like morphology. These phases occurred either as separate plates (Fig. 4a) or formed a cluster containing two crossed plates (Fig. 4b). Plate-like Zr-rich intermetallic phases were present in the microstructure of experimental alloys even after T7 heat treatment with unchanged morphology (Fig. 5a and b). This implies that these phases had high thermal stability, as they were unaffected even at high temperatures during solution heat treatment.

Torn tensile test bars were used for the fracture surface observation. One sample with the best combination of mechanical properties for each experimental alloy with varying Zr addition was selected for the fracture surface evaluation. The structure of Al-Si alloys consists of α (Al) matrix with high plasticity

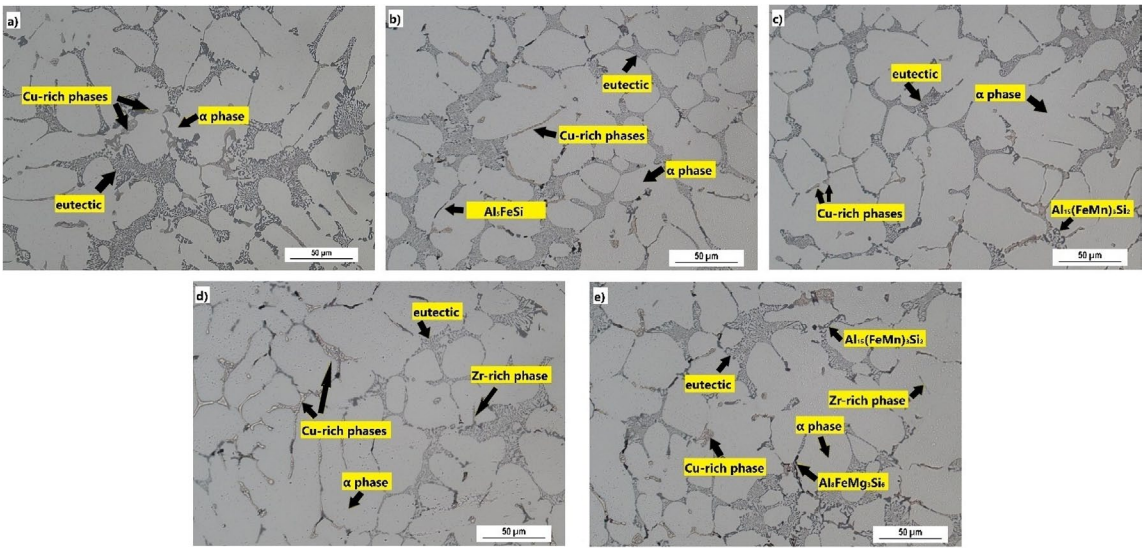

Fig. 2. Microstructure of the experimental alloys depending on the Zr addition (as-cast, H_2SO_4 etch.), addition of: a) 0 wt. % Zr; b) 0.05 wt. % Zr; c) 0.10 wt. % Zr; d) 0.15 wt. % Zr; e) 0.20 wt. % Zr

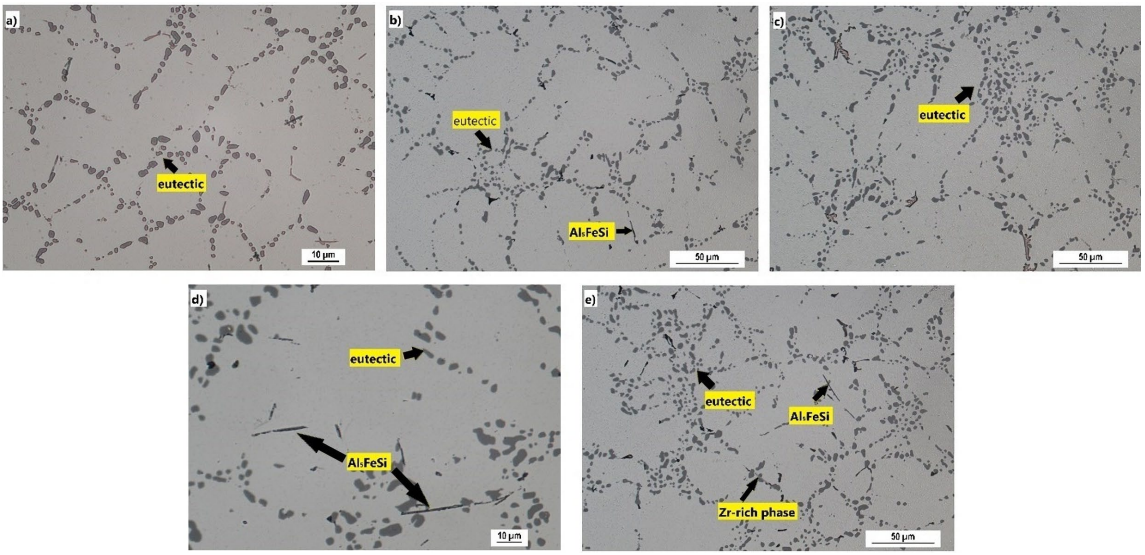

Fig. 3. Microstructure of the experimental alloys depending on the Zr addition (T7, H_2SO_4 etch.), addition of: a) 0 wt. % Zr; b) 0.05 wt. % Zr; c) 0.10 wt. % Zr; d) 0.15 wt. % Zr; e) 0.20 wt. % Zr

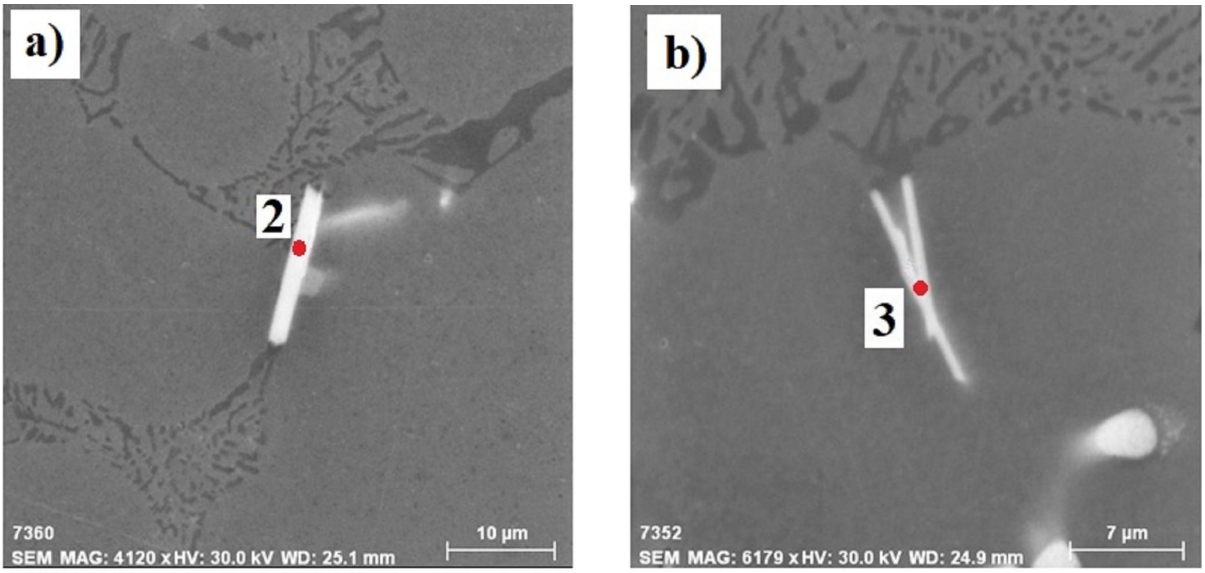

Spectrum: 2

El AN	Series	unn. C [wt.%]	norm. C [wt.%]	Atom. C [at.%]	Error (1 Sigma) [wt.%]
Al 13	K-series	62.23	55.26	71.23	3.16
Si 14	K-series	15.39	13.67	16.93	0.74
Zr 40	K-series	34.98	31.06	11.84	1.32
	Total:	112.60	100.00	100.00	

Spectrum: 3

El AN	Series	unn. C [wt.%]	norm. C [wt.%]	Atom. C [at.%]	Error (1 Sigma) [wt.%]
Al 13	K-series	79.94	68.24	83.73	4.04
Si 14	K-series	4.94	4.21	4.97	0.27
Ti 22	K-series	1.14	0.98	0.68	0.07
Cu 29	K-series	7.32	6.25	3.25	0.24
Zr 40	K-series	23.81	20.33	7.38	0.94
	Total:	117.15	100.00	100.00	

Fig. 4. Morphology of the Zr-rich intermetallic phases in the AlSi5Cu2Mg alloy with corresponding EDX spectrum (as-cast, H_2SO_4 etch.): (a) 0.20 wt. % Zr addition; (b) 0.15 wt. % Zr addition

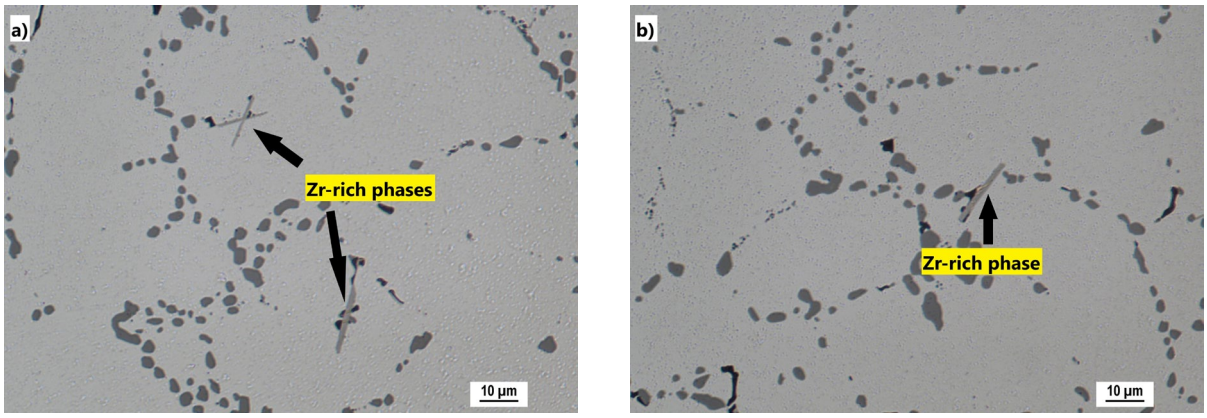

Fig. 5. Detection of the Zr-rich intermetallic phases after T7 (H_2SO_4 etch.): (a) 0.20 wt. % Zr addition, (b) 0.15 wt. % Zr addition

and eutectic Si crystals together with intermetallic phases. The last two mentioned structural components achieve significantly higher hardness together with low plastic properties. The fracture surface appearance is thus determined by the matrix failure mechanism as well as the morphology and size of the eutectic Si and intermetallic phases. In the instance of matrix failure, the transcrystalline ductile fracture mechanism was applied in the experimental alloys. α (Al) matrix fracture mechanism was characterized by the formation of plastically reshaped ridges. The presence of eutectic Si in the modified state was represented on the fracture surface by the formation of dimple morphology. Local occurrence of cleavage facets (Fig. 6) was caused by the cleavage of Cu and Fe intermetallic phases.

The presence of plate-like Zr-rich intermetallic phases was also reflected in the overall character of the fracture surfaces, where it was possible to observe local cleavage of these phases (Fig. 7). Such phases were observed in the vicinity of Fe-rich intermetallic phases. This indicated that Zr phases acted as suitable nucleation sites for further growth of Fe-rich phases.

3.2. Mechanical properties

Mechanical characteristics of the experimental alloys with varying Zr addition obtained after the tensile test in as-cast state and after T7 heat treatment are shown in Figs. 8-11. The

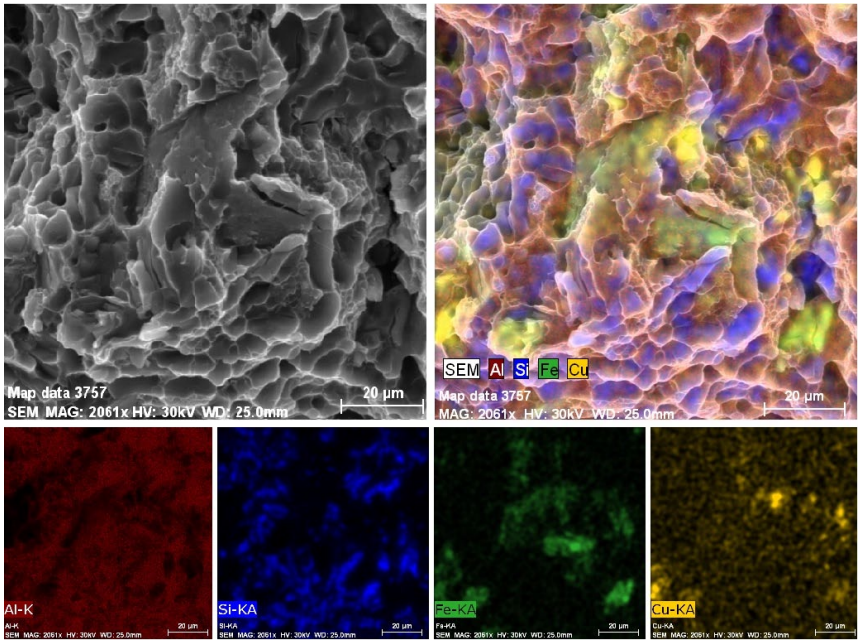

Fig. 6. Fracture surface of the AlSi5Cu2Mg alloy showing Cu and Fe cleavage facets (T7) with EDX mapping of chemical elements

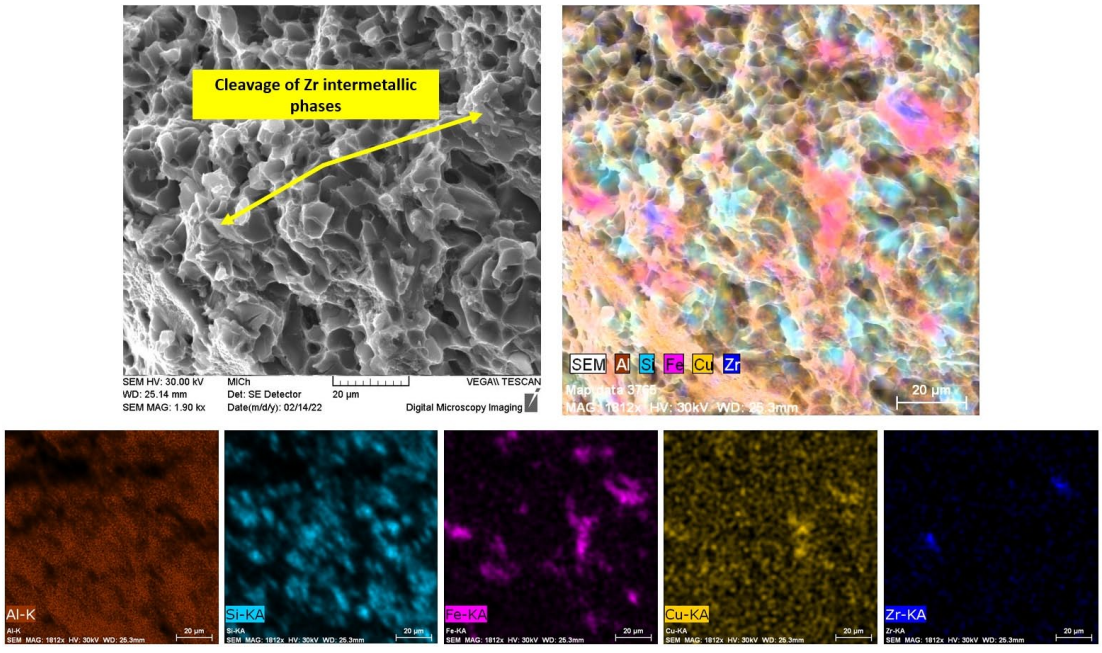

Fig. 7. Cleavage of the Zr-rich intermetallic phases with corresponding EDX mapping of chemical elements

stated values of mechanical properties represent an average of 5 measurements for each experimental alloy. As it can be seen from Figs. 8-11, the addition of Zr did not significantly affect mechanical properties of the experimental alloys in as-cast state. However, compared to the heat-treated experimental alloy without Zr addition, the UTS and YS of the experimental alloys after T7 showed a decrease after the Zr addition. This may have been due to the precipitation of the primary Al_3Zr crystals with tetragonal structure, causing a decrease in mechanical properties. The decrease in mechanical properties was attributed to the insufficient cooling rate during solidification of the experimental alloys, which led to the formation of undesirable primary Al_3Zr crystals. The production of aluminium alloys with addition of zirconium (or other transition elements) requires specific conditions with accelerated cooling to provide complete entry of Zr into the solid solution. This results in the formation of supersaturated solid solution, which subsequently provides an increase in strength characteristics after age hardening. When evaluating the hardness after heat treatment, slight improvement (compared to the heat treated experimental alloy without Zr addition) was documented after the addition of 0.05 and 0.10 wt. % Zr by 6% and after the addition of 0.15 wt. % Zr by 4%. Regardless of the Zr addition, all experimental alloys showed a decrease in ductility from 2% to 1% after T7 heat treatment.

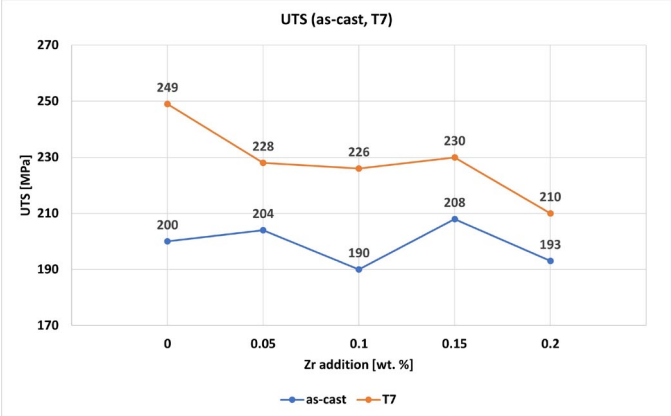

Fig. 8. Impact of varying Zr addition on ultimate tensile strength of the experimental alloys in as-cast and T7 state

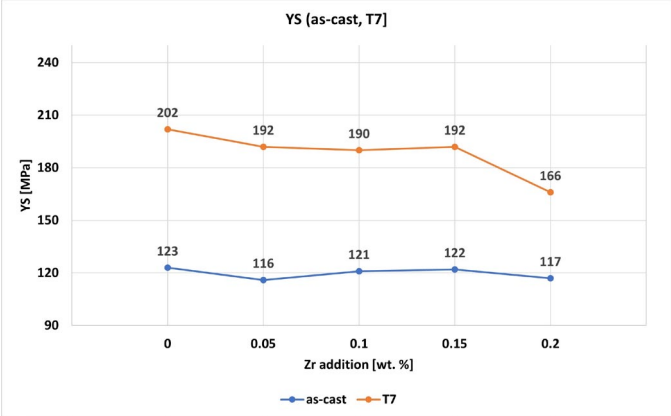

Fig. 9. Impact of varying Zr addition on yield strength of the experimental alloys in as-cast and T7 state

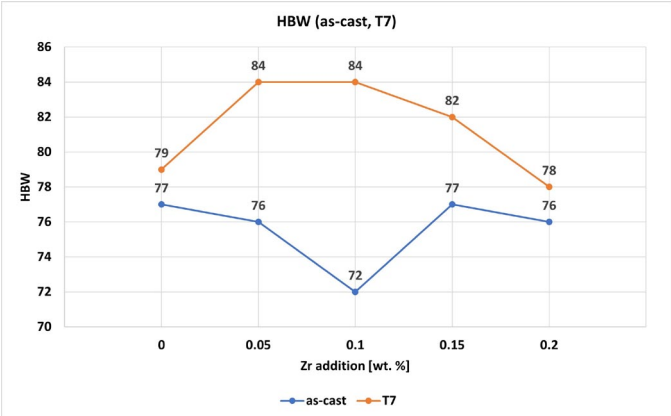

Fig. 10. Impact of varying Zr addition on hardness of the experimental alloys in as-cast and T7 state

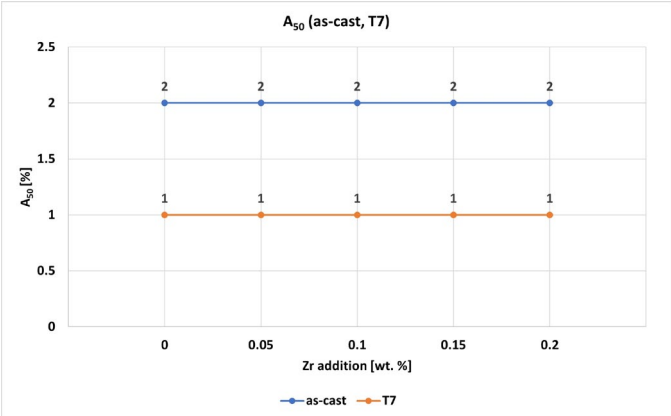

Fig. 11. Impact of varying Zr addition on ductility of the experimental alloys in as-cast and T7 state

3.3. Corrosion behavior

Results of PD tests for the experimental alloys with varying Zr addition in as-cast and heat-treated state are graphically presented in the form of representative PD curves in Fig. 12. Corresponding values of electrochemical characteristics obtained by Tafel analysis of PD curves are presented in TABLE 2. These experiments offered two points of view on measured results: thermodynamics of corrosion given by corrosion potential values E_{corr} and kinetics of corrosion represented by value of corrosion current density i_{corr} [24]. Obtained data showed that applying T7 heat treatment (HT) for the experimental alloy marked as "0" (without Zr addition) improved E_{corr} value to more positive one which points to the higher thermodynamic stability of the alloy after HT. When evaluating the experimental alloys with varying Zr addition, the shift of E_{corr} towards more positive values was observed for as-cast (AC) samples regardless of the Zr addition. This implies that presence of Zr, either in solid solution or as intermetallic phase, contributed to improved thermodynamic corrosion response of the material to corrosive environment. On the other hand, thermodynamic response for the experimental alloys with Zr addition appeared to be worse after HT compared to their AC counterparts. Besides that, E_{corr} values for each HT sample showed that the content or form of Zr presence in the experimental alloys did not play significant role in extent of affecting corrosion thermodynamics as there was no significant difference observed among the HT samples with Zr addition. This trend was observed for AC samples with Zr addition as well. On the other hand, in terms of corrosion kinetics, which is regarded as a more relevant factor when considering the practical usage of the alloy [25], microstructural changes discussed in chapter 3.1 connected with heat treatment led to a suppression of corrosion current density i_{corr}, meaning that corrosion reactions were slower and the experimental alloys degraded less intensively compared to their as-cast counterparts, which was reflected also by lower values of corrosion rate r_{corr} for each HT sample in the particular pair. The i_{corr} results for AC samples also showed that corrosion kinetics was tending to decrease with increasing content of Zr compared to AC samples without Zr addition up to the samples with 0.10 wt. % Zr addition and then it tended to increase with higher Zr addition. However, i_{corr} values for as-cast samples with 0.15 wt. % Zr addition and heat-treated samples with 0.20 wt. % Z addition were still lower compared to the AC alloy without Zr addition, indicating that Zr present in the solid solution is more suitable for corrosion resistance of the experimental alloy. Since the i_{corr} values are directly

proportional to the corrosion rate, Zr addition in carefully chosen range appeared to be rather beneficial for improvement of corrosion resistance of the studied experimental alloys in 3.5% NaCl solution. Similar conclusions were presented also in the study of Kim et al., where authors proposed improved corrosion resistance of 1xxx series Al alloy after addition of Zr in an aggressive salt solution [26]. However, these findings are applied only when comparing the experimental alloys in as-cast state, since the electrochemical values showed that highest corrosion resistance, with regard to i_{corr}, was obtained by the heat-treated sample without Zr addition, showing that T7 heat treatment offered more effective corrosion resistance than the presence of Zr in the experimental alloy.

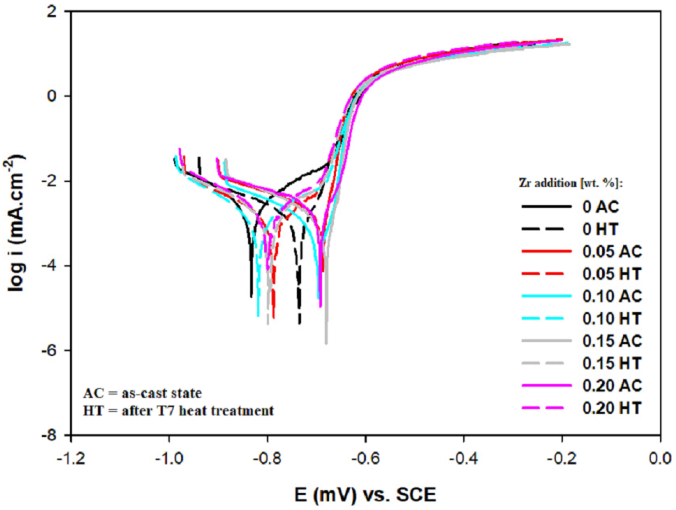

Fig. 12. Potentiodynamic curves measured in 3.5% NaCl for various types of samples

TABLE 2

Electrochemical characteristic obtained by PD tests in 3.5% NaCl for various types of samples

Zr addition [wt. %]	E_{corr} (mV)	i_{corr} (μA.cm^{-2})	β_a (mV/dec.)	β_c (mV/dec.)	r_{corr} (μm.year^{-1})
0 AC	–835	3.51	131	142	0.058
0 HT	–746	0.76	36	171	0.013
0.05 AC	–671	2.81	41	214	0.057
0.05 HT	–784	1.25	101	167	0.021
0.10 AC	–696	1.09	33	152	0.018
0.10 HT	–816	0.89	155	139	0.014
0.15 AC	–685	2.07	31	192	0.273
0.15 HT	–799	1.66	166	157	0.016
0.20 AC	–695	2.28	24	259	0.031
0.20 HT	–798	1.79	155	160	0.025

4. Conclusions

The effect of varying Zr addition on selected properties of the AlSi5Cu2Mg aluminum alloy was studied in this work. The following conclusions can be drawn:

- UTS and YS of the experimental alloys after T7 showed a decrease after the Zr addition. This may have been due to the precipitation of the primary Al_3Zr crystals with tetragonal structure, causing a decrease in mechanical properties. Thus, it can be stated that under the experimental conditions, Zr addition had a deteriorating effect on the mechanical properties.
- The presence of Zr in the experimental alloys with 0.15 and 0.20 wt. % Zr addition resulted in the formation of Zr-rich phases with plate-like morphology. These phases occurred either as separate plates or formed clusters containing two crossed plates. Plate-like Zr-rich intermetallic phases were present in the microstructure of experimental alloys even after T7 heat treatment with unchanged morphology. This implied their high thermal stability at elevated temperatures.
- Fracture surface of the experimental alloy without Zr addition was characterized by transcrystalline ductile fracture with dimple morphology and local occurrence of cleavage facets. The presence of plate-like Zr-rich intermetallic phases was reflected in the overall character of the fracture surfaces, where it was possible to observe local cleavage of these phases.
- Potentiodynamic polarization tests in 3.5% NaCl solution revealed that addition of Zr had a positive effect on thermodynamic corrosion stability of the AlSi5Cu2Mg alloy due to shift of the corrosion potential to a more positive values for all AC samples. Addition of Zr in the AC alloys improved corrosion kinetics by lowering of corrosion current density regardless of the form of its presence in the alloy. Highest corrosion resistance in 3.5% NaCl with regards to corrosion current density was obtained by the alloy without Zr addition in heat-treated state, meaning that heat treatment had more significant impact on the corrosion resistance of the experimental alloys that alloying by Zr.

Acknowledgement

This research was created within the project of the grant agency VEGA 1/0160/22 and Grant System of University of Zilina No. 1/2021 (14862). The authors thank for the support. This paper was also supported under the project of Operational Programme Integrated Infrastructure: Independent research and development of technological kits based on wearable electronics products, as tools for raising hygienic standards in a society exposed to the virus causing the COVID-19 disease, ITMS2014+ code 313011ASK8. The project is co-funding by European Regional Development Fund.

REFERENCES

[1] D. Bolibruchová, M. Žihalová, Arch. Metall. Mater. **59**, 1029-1032 (2014). DOI: https://doi.org/10.2478/amm-2014-0172

[2] D. Bolibruchová, L. Richtárech, S.M. Dobosz, K. Major-Gabryś, Arch. Metall. Mater. **62**, 339-344 (2017). DOI: https://doi.org/10.1515/amm-2017-0051

[3] E. Ozbakir, Ph.D thesis, Development of aluminum alloys for diesel-engine applications, McGill University, Montreal, Canada (2008).

[4] J. Trovao, IEEE Veh. Technol. Mag. **16**, 153-161 (2021). DOI: https://doi.org/10.1109/mvt.2021.3091798

[5] https://www.osti.gov/biblio/1483175-high-performance-cast-aluminum-alloys-next-generation-passenger-vehicle-engines, accessed: 2.6.2022

[6] https://issuu.com/inasport/docs/slevarenstvi_1-2_2020_cele_web, accessed: 3.6.2022

[7] F. Yangyang, Ph.D thesis, Alloying Aluminum with Transition Metals, Worcester polytechnic institute, Worcester, USA (2015).

[8] Ch. Gao, L. Zhang, B. Zhang, Metals **11** (2021). DOI: https://doi.org/10.3390/met11020357

[9] A.R. Farkoosh, Ph.D thesis, Development of Creep-Resistant Al-Si Alloys Strengthened with Nanoscale Dispersoids, Mining and Materials Engineering, Montreal, Canada (2014).

[10] A.R. Farkoosh, X.G. Chen, M. Pekguleryuz, Mater. Sci. Eng. A. **620**, 181-189 (2015). DOI: https://doi.org/10.1016/j.msea.2014.10.004

[11] K.E. Knipling, D.C. Dunand, D.N. Seidman, Z. Metallk. **97**, 246-265 (2006). DOI: https://doi.org/10.3139/146.101249

[12] https://www.semanticscholar.org/paper/Zirconium-Solubility-in-Aluminum-Alloys-Muddle-Sigli/1a3d2aa5d17956c40fa5320d794df851e132af12, accessed: 10.6.2022

[13] P.D. Staublin, MSc. thesis, Investigationg Microalloying Elements to Accelerate Zirconium Trialuminide Precipitation in Aluminum Alloys, Michigan Technological University, Michigan, USA (2019).

[14] F. Wang, D. Qiu, Z. Liu, J. Taylor, M. Easton, M. Zhang, Acta Mater. **15**, 5636-5645 (2013). DOI: https://doi.org/10.1016/j.actamat.2013.05.044

[15] M. Rahiman, S. Amirkhanlou, P. Blake, S. Ji, Mat. Sci. Eng. A. **721**, 328-338 (2018). DOI: https://doi.org/10.1016/j.msea.2018.02.060

[16] F. Wang, D. Qiu, J. Taylor, M. Easton, M. Zhang, Trans. Nonferrous Met. Soc. China **24**, 2034-2040 (2014). DOI: https://doi.org/10.1016/S1003-6326(14)63309-4

[17] A.M. Samuel, S.S. Mohamed, H.W. Doty, S. Valtierra, F.H. Samuel, Int. J. Cast Met. Res. **32**, 46-58 (2018). DOI: https://doi.org/10.1080/13640461.2018.1518662

[18] W. Bevilaqua, A. Standtlander, A. Froehlich, G. Braga, A. Reguly, Mater. Res. Express. **7**, 026532 (2020). DOI: https://doi.org/10.1088/2053-1591/ab7163

[19] G. Liu, P. Blake, S. Ji, J. Alloys Compd. **809**, 151795 (2019). DOI: https://doi.org/10.1016/j.jallcom.2019.151795

[20] S.K. Shaha, F. Czerwinski, D. Chen, Metall. Mater. Trans. A. **46**, 3063-3078 (2015). DOI: https://doi.org/10.1007/s11661-015-2880-x

[21] E. Sjolander, S. Seifeddine, J. Matter. Process. Technol. **210**, 1249-1259 (2010). DOI: https://doi.org/10.1016/j.jmatprotec.2010.03.020

[22] D. Kajánek, F. Pastorek, S. Fintová, A. Bača, Procedia Eng. **192**, 399-403 (2017). DOI: https://doi.org/10.1016/j.proeng.2017.06.069

[23] B. Hadzima, D. Kajánek, M. Jambor, J. Drábiková, M. Březina, J. Buhagiar, J. Pastorková, M. Jacková, Metals **10** (2020). DOI: https://doi.org/10.3390/met10111521

[24] M. Mhaede, F. Pastorek, B. Hadzima, Mater. Sci. Eng. C. **39**, 330-335 (2014). DOI: https://doi.org/10.1016/j.msec.2014.03.023

[25] E. Ghali, Corrosion Resistance of Aluminum and Magnesium Alloys: Understanding, Performance, and Testing, Wiley, New Jersey, 2010.

[26] Y. Kim, J. Park, B. An, Y. Lee, Ch. Yang, J. Kim, Materials **11** (2018). DOI: https://doi.org/10.3390/ma11101982